RSC Advances

PAPER

View Article Online
View Journal | View Issue

Cite this: *RSC Adv.*, 2022, **12**, 22623

Preparation and study of the flame retardant properties of C_{60}/PMMA microspheres

Lanjuan Xu,[ab] Juncheng Jiang, *[ac] Lei Ni,[a] Zhiquan Chen[a] and Chao Li[ab]

Received 13th June 2022
Accepted 22nd July 2022

DOI: 10.1039/d2ra03642h

rsc.li/rsc-advances

In this paper, highly flame retardant C_{60}/PMMA composites were prepared using an *in situ* polymerization method by introducing fullerene (C_{60}) into polymethyl methacrylate (PMMA) to improve its combustion characteristics. The apparent morphologies of PMMA and C_{60}/PMMA microspheres were observed by scanning electron microscopy (SEM), and the structure was characterized by infrared spectroscopy (FT-IR). The thermal stability and flame retardancy were characterized using a synchronous thermal analyzer, a cone calorimeter and an oxygen index tester. The results show that the maximum initial decomposition temperature of C_{60}/PMMA-2 (prepared using C_{60} with a concentration of 2 mg mL^{-1}) is 234.89 °C, which is about 59.89 °C higher than that of PMMA, and the thermal stability is the best. The limiting oxygen index of the C_{60}/PMMA-2 composite is 21.8, which is 28.2% higher than that of pure PMMA. In addition, the peak heat release rate (PHRR) of C_{60}/PMMA is reduced by 630.4 kW m^{-2} when compared with pure PMMA, which means that the flame retardant property is improved. Meanwhile, the mechanical properties of the PMMA are also improved by adding C_{60}.

1 Introduction

Methyl methacrylate (PMMA) is an important general polymer with excellent properties such as high transparency, low cost, high mechanical strength, easy operation and processing, and chemical corrosion resistance.[1,2] It is usually used as a substitute for glass and is widely used in various fields. However, the wide application of PMMA is limited due to its brittleness, poor thermal stability, easy combustion, and poor impact resistance.[3] In recent years, many attempts have been made to improve the performance of PMMA. Among many methods, using nano-materials as flame retardants to modify polymers is an important route, which can not only achieve a high level of flame retardancy, but also maintain and strengthen the mechanical properties of the matrix.[4,5] The application of nano-materials in PMMA composites is a hot research topic.

Carbon materials are widely used as flame retardants because of their excellent flame retardancy and environmentally friendliness.[6,7] For example, graphene and carbon nanotubes can significantly improve the thermal stability of polymer materials, reduce the heat release rate during combustion, delay the combustion process, and improve the physical and mechanical properties of polymers.[8–10] Therefore, the introduction of carbon materials into PMMA as flame retardants is feasible. Dai[11] *et al.* prepared (graphene oxide) GO/PMMA and (pentafluorophenyl functional graphene) PFP-f-graphene/PMMA composites by solution blending method. Studies have shown that compared with pure PMMA, the tensile strength of PMMA modified by two kinds of graphene is improved, and it is found that the modified PFP-f-graphene is more effective to improve the mechanical properties of PMMA. Dittrich[12] *et al.* prepared a polypropylene/multi-wall carbon nanotube composite by melt blending, and found that with the continuous addition of carbon nanotubes, the initial thermal decomposition temperature and maximum thermogravimetric temperature of the composite material system have been increased, and the thermal stability has been improved. Zuo[13] *et al.* polyimide (PI) composite aerogels with enhanced flame retardant properties were prepared using freeze-drying methods by adding environmentally friendly flame retardant additives (*i.e.*, graphene and montmorillonite), and it is found that there is a strong interaction between the two components, and the graphene oxide/MMT hybrid can be dispersed in water synergistically to enhance the mechanical properties, thermal stability and flame retardancy of the composite aerogel. Veerendra[14] prepared three-dimensional flame retardant carbon–carbon nanotubes mixed foam. It was found that the addition of three-dimensional flame retardant carbon–carbon nanotubes in phenolic resin could not only improve the compressive strength (6.5 MPa), but also improve the thermal stability and flame retardant performance. Wang[15] *et al.* used *in situ* polymerization method to prepare PMMA/carbon nanotubes (CNTs) composites, and explored the influence of CNTs on PMMA process. The results showed that CNTs not only improved the

[a]*College of Safety Science and Engineering, Nanjing Tech University, Nanjing, Jiangsu, China, 210009*

[b]*College of Chemical Engineering and Safety, Binzhou University, Binzhou, Shandong, China, 256600*

[c]*School of Environment and Safety Engineering, Changzhou University, Changzhou, Jiangsu, China, 213164*

thermal stability of PMMA, but also greatly improved the flame retardant properties and reduced the fire risk of PMMA materials. Jia[16] *et al.* prepared a new type of high impact polystyrene (HIPS)/k-APP/COOH-MWCNTs composites by melt blending method. Experiments show that k-APP and COOH-MWCNTs have synergistic effect, improve the thermal stability of the composites, and improve the limiting oxygen index of the material. Xing[17] *et al.* prepared functionalized multi-walled carbon nanotubes (DPPA-MWCNT) by the reaction of A-MWCNT (aminated multiwalled carbon nanotubes) with diphenylphosphine chloride (DPP-Cl). The strong flame retardancy of DPPA-MWCNT is attributed to the barrier effect of carbon nanotubes, which can provide sufficient time for DPPA-MWCNT and its functional groups to capture and degrade polymer radicals, thus catalyzing coking. Wang[18] *et al.* synthesized manganese–cobalt oxide/graphene hybrid ($MnCo_2O_4$-GNS). The cone test results had showed that peak HRR and SPR values of $MnCo_2O_4$-GNS/PBT composites were lower than that of pure PBT and Co_3O_4-GNS/PBT composites. They also found that the incorporation of $MnCo_2O_4$-GNS hybrids gave rise to apparent decrease of pyrolysis products containing aromatic compounds, carbonyl compounds, carbon monoxide and carbon dioxide, attributed to combined impact of physical barrier for graphene and cat O_4 for organic volatiles and carbon monoxide. Fullerene (C_{60}) is a new carbon material with unique football-like and three-dimensional structure, which is considered to be one of the most promising nano-additives.[19–21]

Fullerene (C_{60}) can greatly improve the dispersion of nanofillers in polymer matrix due to its better dispersibility than carbon nanotubes (CNTs) and carbon nanofibers (CNF).[22] It can also capture macromolecular free radicals, inactivate free radicals, form lower active substances, so as to improve the thermal stability of composites. At the same time, the formation of a viscous insulating carbon layer on the surface of the material by C_{60} will inhibit the thermal degradation reaction and improve the flame retardancy of the composite.[23–25] However, the research heat of carbon materials is mainly concentrated on graphene and carbon nanotubes, and there are few reports on fullerene as a flame retardant.

In this paper, carbon material fullerene (C_{60}) was introduced to improve the combustion characteristics of polymethyl methacrylate (PMMA) by *in situ* polymerization, and a high flame retardant microspheric C_{60}/PMMA composite was successfully prepared. The apparent morphologies of PMMA and C_{60}/PMMA microspheres were observed by optical microscope and scanning electron microscope. The compositions of materials were analyzed by infrared spectroscopy. The thermal stability and flame retardant properties were characterized by synchronous thermal analyzer, oxygen index tester, and cone calorimeter. In addition, the flame-retardant mechanism of C_{60} on PMMA was investigated.

2 Experimental

2.1 Materials

Methyl methacrylate (PMMA), polyvinyl alcohol (PVA), azobisisobutyronitrile (AIBN), and fullerene (C_{60}), were purchased from Shanghai McLin Biochemical Technology Co., Ltd. Sulfuric acid (H_2SO_4, analysis pure) was purchased from Yantai Far East Fine Chemical Co., Ltd. Sodium nitrate ($NaNO_3$) was provided by Tianjin Kaitong Chemical reagent Co., Ltd. Potassium permanganate ($KMnO_4$) was purchased from Jintan Experimental Factory, Shanghai Institute of Chemical Industry. Hydrogen peroxide (H_2O_2) was purchased from Huainan Zhongcheng Chemical Co., Ltd.

2.2 Preparation of C_{60}/PMMA composite

As shown in Fig. 1, the treated fullerene powder was prepared into 1 mg mL^{-1}, 2 mg mL^{-1} and 3 mg mL^{-1} uniform aqueous solutions by ultrasonic oscillation. Similar with the preparation method of PMMA microspheres, 40 g distilled water was replaced by 10 g fullerene solution and 30 g distilled water, the amount of azobisisobutyronitrile (AIBN) was increased to 0.26 g, and the reaction time was 30 min. Finally, the product was filtered and dried to obtain high flame retardant C_{60}/PMMA microspheres.

2.3 Instruments and measurements

The apparent morphologies of PMMA and C_{60}/PMMA microspheres were observed by a scanning electron microscopy (Hitachi SU8010, Japan). Fourier transform infrared spectroscopy spectra were recorded on a FT-IR (Nicolet 380, Germany). Thermal stability of PMMA and its composites were tested by a synchronous thermal analyzer (STA449F3, Germany). Flame retardant properties of the materials were measured by an oxygen index tester (SH5706A, China) and a cone calorimeter (FTT Standard Cone Calorimeter, UK). Raman spectra of the carbon residues were tested with a Raman spectrometer (HORIBA HR Evolution, France). A Gel permeation chromatograph (Waters Alliance E2695, USA) was used to study the effect of C_{60} on the molecular weight of PMMA. In order to study the effect of C_{60} on the transmittance of PMMA, the UV/NIR spectra were measured by a UV-Vis spectrophotometer (Lambda 750, China). Mechanical properties of the materials were tested by an electronic universal testing machine (WDW 50 M, China).

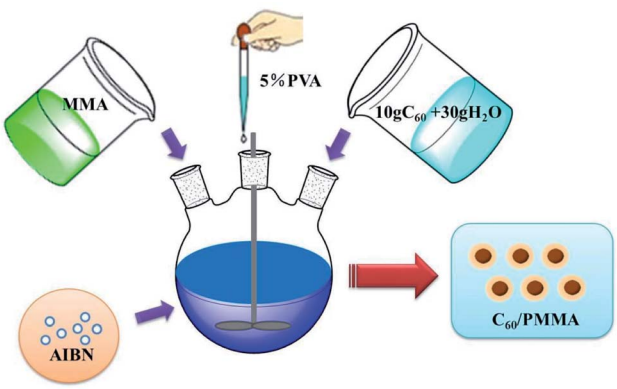

Fig. 1 Preparation diagram of C_{60}/PMMA composite.

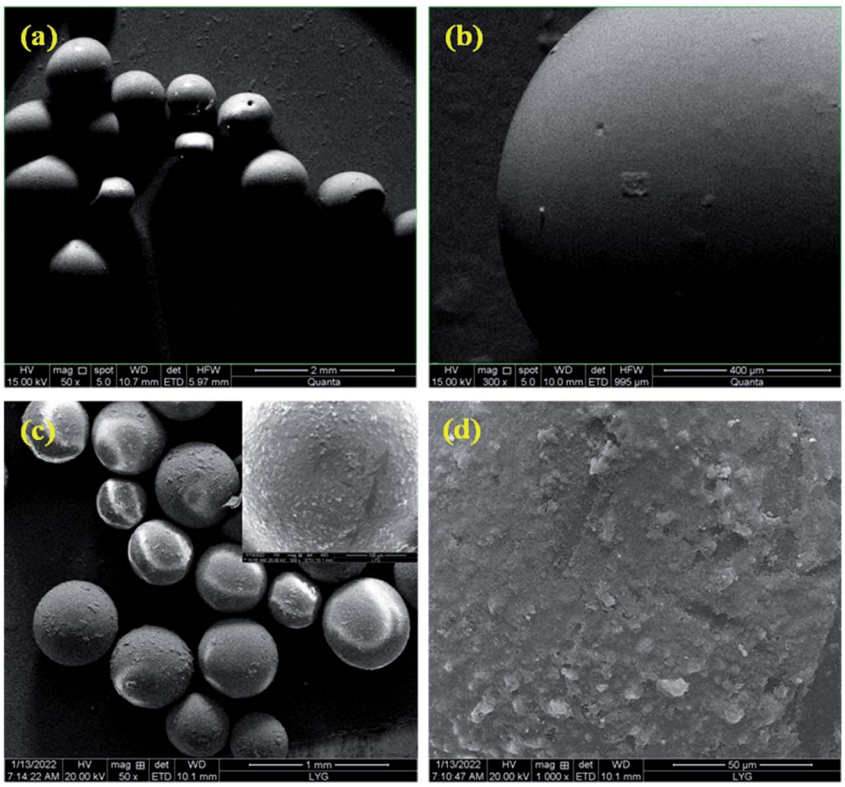

Fig. 2 SEM images of composite material. (a), (b) PMMA, (c) and (d)C_{60}/PMMA composite material.

3 Results and discussion

3.1 Scanning electron microscope (SEM)

SEM images of PMMA and C_{60}/PMMA composite are shown in Fig. 2.

It can be observed from Fig. 2(a) and (b) that the prepared PMMA microspheres are uniform, most of which have smooth surface. Strangely, some of the microspheres have holes in them, which may be due to the high temperature in the polymerization process that destroys the internal chemical bonds, and the reaction stops before materials becoming spherical. It can be seen from Fig. 2(c) and (d) that C_{60}/PMMA composites are spherical, with rough surfaces, which means that C_{60} is evenly attached to the surface of PMMA.

3.2 Fourier transform infrared (FT-IR) spectrometer

Fig. 3 shows the FTIR spectra of PMMA and C_{60}/PMMA microspheres prepared with different concentrations of fullerene aqueous solution (1 mg mL^{-1}, 2 mg mL^{-1} and 3 mg mL^{-1}, denoted as C_{60}/PMMA-1, C_{60}/PMMA-2 and C_{60}/PMMA-3, respectively).

PMMA has the stretching vibration peak of O–H at 3470 cm^{-1}, the characteristic absorption peak of ester group at 1740 cm^{-1}, the bending vibration of C–H at 1430 cm^{-1}, 1320 cm^{-1} and 1160 cm^{-1}, which means there are ester groups and no benzene ring in it. The infrared spectrum of C_{60} shows that there is a stretching vibration absorption peak of C=C at 1640 cm^{-1}, and the hydroxyl absorption peak of C_{60} is significantly wider at 3420 cm^{-1} after oxidation. It can be found in the amplification diagram at 3300–3650 cm^{-1} that the number of C_{60} absorption peaks after oxidation increased and the peak value increased, indicating that the oxygen-containing groups of C_{60} after oxidation increased. Beside the same characteristic absorption peaks with PMMA, C_{60}/PMMA-1, C_{60}/PMMA-2, and

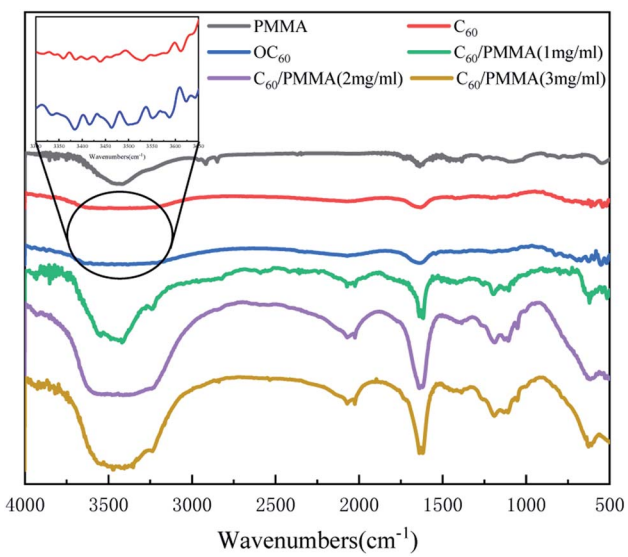

Fig. 3 Fourier infrared spectrum of composite materials.

C_{60}/PMMA-3 all have a stretching vibration peak of C=C at 1640 cm^{-1}, which indicates that the material on the surface of PMMA is fullerene (C_{60}).

3.3 Thermogravimetric analysis (TGA)

The TGA/DTG curves are shown in Fig. 4, and the corresponding data are listed in Table 1.

It can be seen from Table 1 that the initial decomposition temperature (T_{onset}) and the maximum decomposition temperature (T_{max}) of C_{60}/PMMA composites are all higher than that of PMMA, and the amount of char residues at 500 °C is also increased with the addition of C_{60}, which indicates that C_{60} can improve the thermal stability of composites. On the one hand, C_{60} has excellent thermal stability and good thermal conductivity, which can transfer the heat required for thermal decomposition of composites in time. On the other hand, C_{60} can form a viscous insulating carbon layer on the surface when the composite is heated, which inhibits the thermal degradation reaction, and improves the flame retardancy of the material. In addition, the initial decomposition temperature of C_{60}/PMMA-3 is lower than that of C_{60}/PMMA-2, which may be due to the uneven dispersion of C_{60} in the PMMA matrix when the addition amount is too large. However, the maximum thermal degradation rates of C_{60}/PMMA composites are lower than that of pure PMMA, which is because the accumulated internal heat is rapidly released after the carbon layer formed by C_{60} decomposes.

3.4 Flame retardant performance analysis

As shown in Table 2, the LOI values of PMMA, C_{60}/PMMA-1, C_{60}/PMMA-2 and C_{60}/PMMA-3 samples are calculated respectively. According to the results, the oxygen indexes of C_{60}/PMMA-1 (20.4), C_{60}/PMMA-2 (21.8), and C_{60}/PMMA-3 (21.2) are 20.0%, 28.2%, and 24.7% higher than that of PMMA, respectively, which demonstrates that the addition of C_{60} increases the minimum oxygen concentration required for combustion of PMMA, especially when the concentration of C_{60} is 2 mg mL^{-1}.

For further evaluation of the flame retardant property, heat release rate (HRR) and total heat release (THR) of polymers must be tested.[26,27] The HRR curves of composite materials are shown in Fig. 5(a). It can be seen that the peak heat release rate (PHRR) of C_{60}/PMMA-3 is 440.4 kW m^{-2}, which is 630.4 kW m^{-2} lower than that of PMMA (964.1 kW m^{-2}). As shown in Fig. 5(b), the maximum heat release of pure PMMA can be as high as 97.2 MJ m^{-2}. With the addition of C_{60}, THR of PMMA is decreased. The THR of C_{60}/PMMA-3 is 45.1 MJ m^{-2}, which is 53.6% lower than that of pure PMMA.

According to the above results, it can be concluded that the addition of C_{60} can significantly reduce the LOI, PHRR and THR values of PMMA, indicating that it is an effective flame retardant. After the composite material is ignited, the material burns and releases a lot of heat. During this period, C_{60} forms a carbon layer on the surface of the matrix. The thermal conductivity of the carbon layer is poor, which can block the destruction of the material matrix, resulting in the reduction of the heat release rate of the material.

Table 1 Data of thermogravimetric analysis

Sample	T_{onset} °C	T_{max} °C	U_{max}%/min	Amount of char residues (500 °C) wt%
PMMA	175	253.99	8.12	0.60
C_{60}/PMMA-1	208	371.07	9	0.81
C_{60}/PMMA-2	234.89	372.89	9.41	0.97
C_{60}/PMMA-3	221.87	389.31	8.4	1.95

Table 2 LOI test results of PMMA and its composites

Number	Sample	C_{60} addition	LOI (%)	Average value
1	PMMA	0	17.0	17.0
2			16.9	
3			17.1	
4	C_{60}/PMMA-1	1 mg mL^{-1}	20.1	20.4
5			20.5	
6			20.7	
7	C_{60}/PMMA-2	2 mg mL^{-1}	21.9	21.8
8			21.6	
9			22.0	
10	C_{60}/PMMA-3	3 mg mL^{-1}	21.3	21.2
11			21.4	
12			20.9	

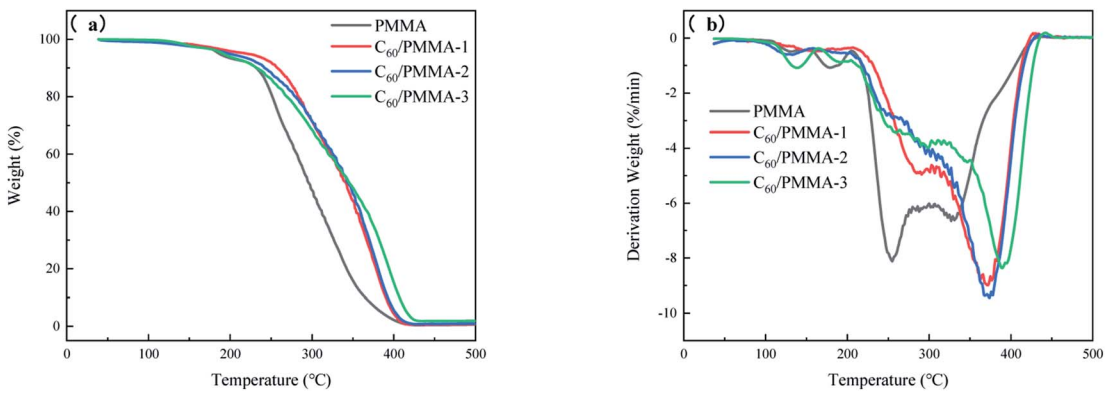

Fig. 4 (a) TGA and (b) DTG curves of composite materials.

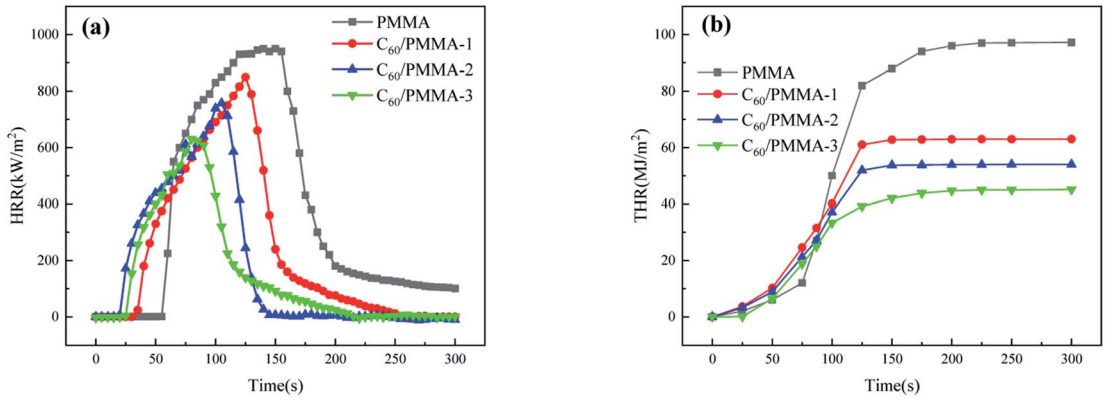

Fig. 5 (a) HRR and (b) THR curves of composite materials.

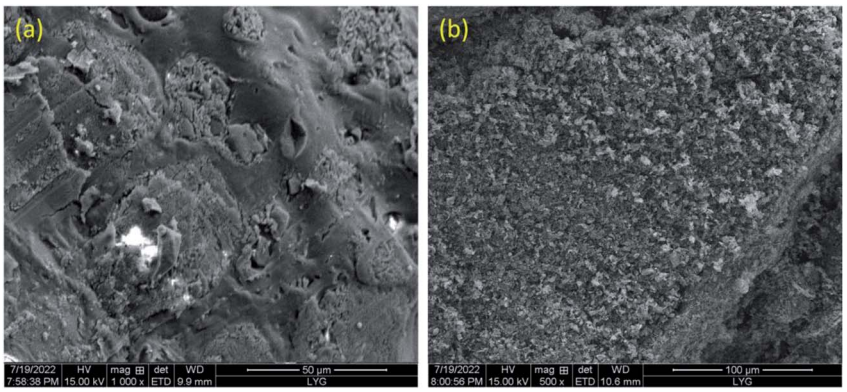

Fig. 6 SEM images of residues after combustion test(a) PMMA, (b) C_{60}/PMMA-3.

3.5 Analysis of the flame retardant mechanism

Fig. 6 shows the SEM images of samples after combustion test. It can be seen from Fig. 6(a) that the burned PMMA is loose in texture, rough in surface. In comparison, the surface cracks of burned C_{60}/PMMA-3 (Fig. 6(b)) are significantly reduced, and the density is correspondingly increased, which enhances the heat and mass insulation effect of carbon layer, and then significantly improves the flame retardancy of PMMA. The dense carbon layer generated by C_{60} effectively hinders the further combustion of the material, which is consistent with the results of HRR analysis.

Fig. 7 shows the Raman spectra of the carbon residues for PMMA and C_{60}/PMMA-3. The vibration of disordered carbon and graphite carbon was detected near 1342 cm^{-1} and 1558 cm^{-1}, corresponding to D-band and G-band in the figure, respectively. Generally, the ratio of peak strengths of D-band and G-band ($R = I_D/I_G$) is used to estimate the graphitization degree of residual carbon. The lower the R, the higher the graphitization degree and the better the thermal stability. It can be seen from Fig. 7 that the R value of PMMA is 0.95, while that of C_{60}/PMMA-3 is 0.9, which indicates that the addition of C_{60} is conducive to the formation of graphitized carbon, and thus making the carbon layer more stable.

As shown in Fig. 8, C_{60} can form a viscous insulating carbon layer on the surface of the material, preventing the transfer of oxygen and heat from being transferred to the interior, and reducing of volatiles generated by the thermal decomposition of PMMA.[28,29] In addition, C_{60} can capture the free radicals

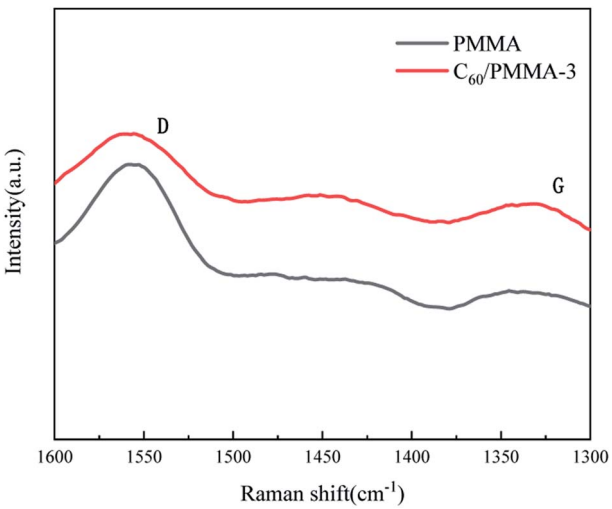

Fig. 7 Raman spectra of the carbon residues after combustion test.

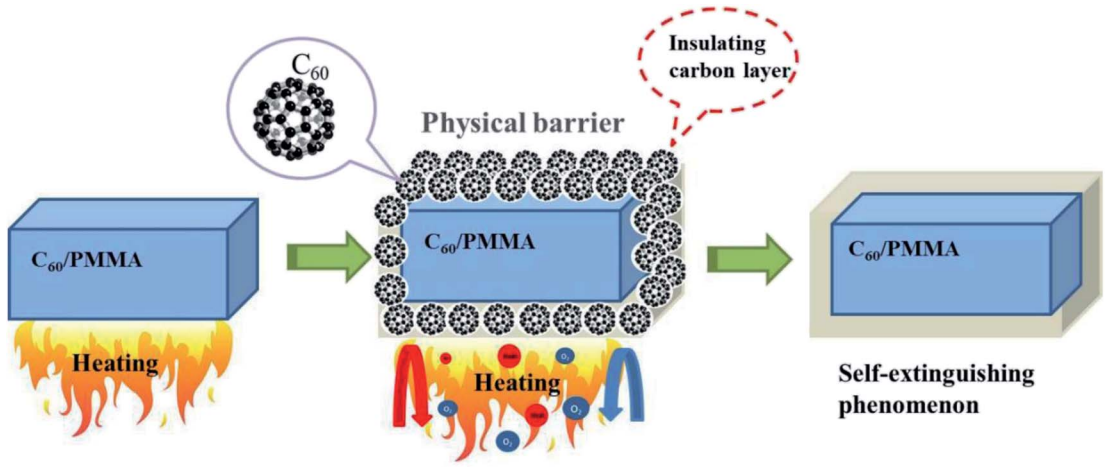

Fig. 8 Flame retardant mechanism diagram.

generated during the thermal degradation of PMMA, especially oxygen-containing free radicals, and each C_{60} molecule can react with multiple free radicals, which can delay the material combustion.[30,31]

3.6 Molecular weight test

The number average molecular weight (M_n) and weight average molecular weight (M_W) of the samples are listed in Table 3.

As shown in Table 3, the molecular weight of C_{60}/PMMA is significantly higher than that of pure PMMA. When the amount of C_{60} added in the polymerization reaction is small (C_{60}/PMMA-1, C_{60}/PMMA-2), it is evenly dispersed, and the hindrance to the formation of long chain is small, so the molecular weight is higher. When the amount of C_{60} is large (C_{60}/PMMA-3), its agglomeration effect will affect the polymerization of MMA monomer, which reduces the degree of polymerization to a certain extent, resulting in the reduction of molecular weight.

3.7 Transmittance analysis

Fig. 9 shows the UV-Vis spectra of pure PMMA and C_{60}/PMMA composites. It can be seen that the transmittance of PMMA in the visible wavelength range (420–780 nm) is 91%. With the addition of C_{60}, the transmittance of PMMA decreased. Compared with pure PMMA, the maximum decrease was about 18.6% (C_{60}/PMMA-3).

3.8 Analysis of mechanical properties

As shown in Fig. 10, the tensile strength and elastic modulus of PMMA are 54.2 MPa and 1865.3 MPa, respectively. Compared

Table 3 Molecular weight for PMMA and its composites

Sample	M_n (g mol^{-1})	M_w (g mol^{-1})
PMMA	26 543	38 604
C_{60}/PMMA-1	41 254	78 261
C_{60}/PMMA-2	48 529	85 635
C_{60}/PMMA-3	31 214	53 428

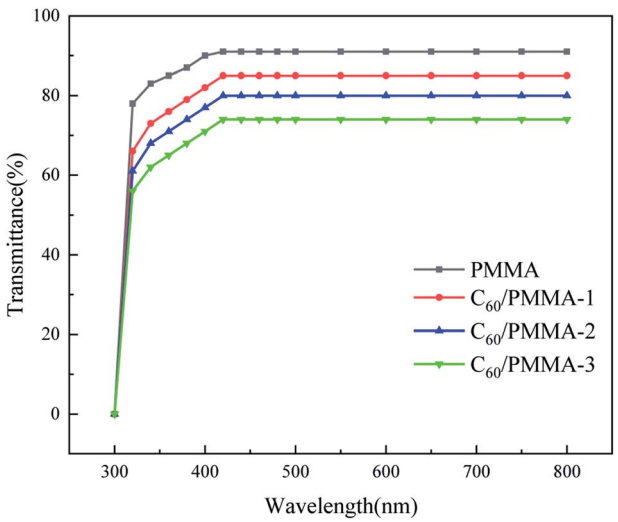

Fig. 9 Ultraviolet-visible (UV-vis) spectra of composite materials.

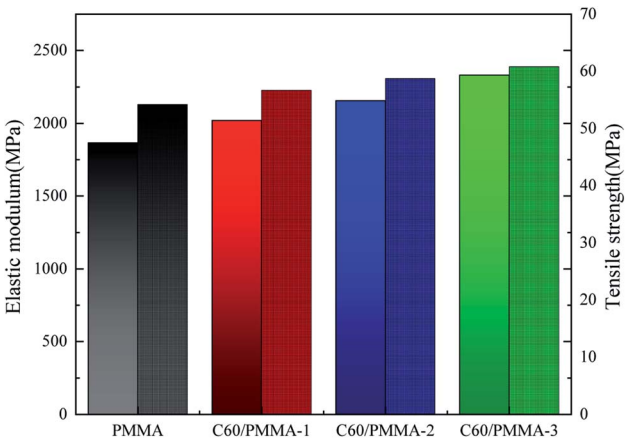

Fig. 10 Elastic modulus and tensile strength of composite materials. (The one with the mottling pattern is tensile strength and the other is elastic modulus).

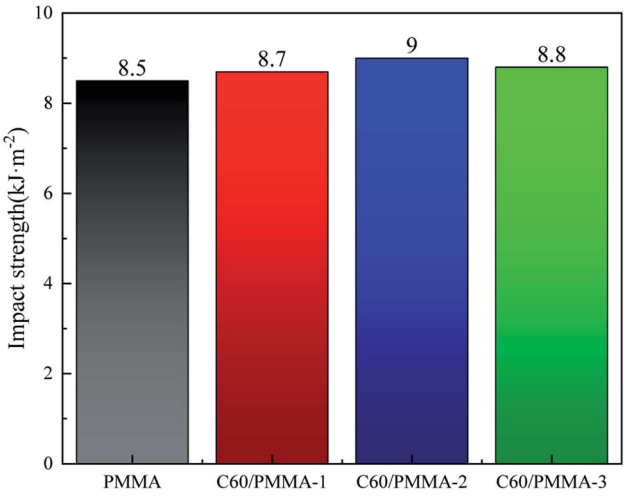

Fig. 11 Impact strength of composite materials.

with pure PMMA, the strength and elastic modulus of C_{60}/PMMA composites prepared with 3 mg mL^{-1} C_{60} (C_{60}/PMMA-3) are the highest (60.8 MPa, 2330.5 MPa), which are increased by 12.1% and 24.9%, respectively. This may be due to the network structure formed by C_{60} in the PMMA matrix, which can improve the interaction between molecular chains and enhance the tensile property of materials.

The impact strength was also tested. It can be seen from Fig. 11 that the notch-free impact strength of C_{60}/PMMA composites increases first and then decreases. Compared with PMMA, the impact strength of C_{60}/PMMA-2 is increased by 5.8%. This is because the addition amount of C_{60} is appropriate, which makes it well dispersed in PMMA and thus the energy absorption effect is better. However, with the increase of C_{60} amount, local agglomeration occurs, and the absorption ability of impact energy is destroyed, so the impact strength of C_{60}/PMMA-3 decreases.

4 Conclusion

In this paper, a high flame retardant C_{60}/PMMA microsphere is successfully prepared by the *in situ* polymerization method. Due to the addition of C_{60}, increases of the limiting oxygen index and initial decomposition temperature as well as decreases of the peak heat release rate (PHRR) and total heat release (THR) are observed. Unlike other flame retardants, mechanical properties of the materials are also improved by C_{60}. When the concentration of C_{60} is 2 mg mL^{-1}, thermal stability and impact strength of the C_{60}/PMMA composite are the best, which is because C_{60} is well dispersed in the PMMA matrix. However, the transmittance of PMMA decreases with the addition of C_{60}, which makes the C_{60}/PMMA composite cannot be used in situations requiring high transparency.

Conflicts of interest

We declare that we have no conflict of interest.

Data availability statement

The raw data required to reproduce these findings cannot be shared at this time as the data also forms part of an ongoing study.

Acknowledgements

The authors are grateful for the reviewers' instructive suggestions and careful proofreading. This work was supported by the National Natural Science Foundation of China (Nos. 51834007 and 21927815).

References

1 W. S. Wang, C. K. Liang, Y. C. Chen, Y. L. Su, T. Y. Tsai and Y. W. Chen-Yang, Transparent and flame retardant PMMA/clay nanocomposites prepared with dual modified organoclay, *Polym. Adv. Technol.*, 2012, **23**(3), 625–631.
2 A. F. Robin, K. Stoeffler, B. Ashrafi, Y. Zhang and B. Simard, Large-Scale Production of PMMA/SWCNT Composites Based on SWCNT Modified with PMMA, *ACS Appl. Mater. Interfaces*, 2012, **4**(4), 1990–1997.
3 S. Kim and C. A. Wilkie, Transparent and flame retardant PMMA nanocomposites, *Polym. Adv. Technol.*, 2008, **19**(6), 496–506.
4 X. Wang, W. Guo, W. Cai, J. Wang and Y. Hu, Recent advances in construction of hybrid nano-structures for flame retardant polymers application, *Applied Materials Today*, 2020, **20**(25), 100762.
5 A. Ct, Z. Shuai, C. Tz, B. Zf and B. Hl, Highly fibrillated and intrinsically flame-retardant nanofibrillated cellulose for transparent mineral filler-free fire-protective coatings, *Chem. Eng. J.*, 2021, **419**(5), 129440.
6 S. C. Lao, J. H. Koo, T. J. Moon, M. Londa, C. C. Ibeh, G. E. Wissler and L. A. Pilato, Flame-retardant polyamide 11 nanocomposites: further thermal and flammability studies, *J. Fire Sci.*, 2011, **29**(6), 479–498.
7 X. Wang, E. N. Kalali, J. T. Wan and D. Y. Wang, Carbon-family materials for flame retardant polymeric materials, *Prog. Polym. Sci.*, 2017, **69**, 22–46.
8 Z. Wang, C. Soutis and M. Gresil, Fracture toughness of hybrid carbon fibre/epoxy enhanced by graphene and carbon nanotubes, *Appl. Compos. Mater.*, 2021, **28**(4), 1111–1125.
9 Y. Song, B. Xue, J. Wang, R. Qin and M. Niu, Ammonium polyphosphate wrapped carbon microspheres: a novel flame retardant with smoke suppression for poly (ethylene terephthalate), *J. Polym. Res.*, 2020, **27**(1), 1–12.
10 Z. He, Z. Zhao, S. Xiao, J. Yang and M. Zhong, Preparation of carbon-based hybrid particles and their application in microcellular foaming and flame-retardant materials, *RSC Adv.*, 2018, **8**(47), 26563–26570.
11 J. Dai and M. Lang, Preparation and mechanical properties of graphene oxide/PMMA and surface functionalized graphene/PMMA composites, *Acta Chim. Sin.*, 2012, **70**(11), 1237–1244.

12 B. Dittrich and K. A. Wartig, Flame retardancy through carbon nanomaterials:Carbon biack,multiwall nanotubes,expanded graphite,multi-layer graphene and graphene in polypropylene, *Polym. Degrad. Stab.*, 2013, **98**(8), 1495–1505.

13 L. Zuo, W. Fan, Y. Zhang, L. Zhang, W. Gao, Y. Huang and T. Liu, Graphene/montmorillonite hybrid synergistically reinforced polyimide composite aerogels with enhanced flame-retardant performance, *Compos. Sci. Technol.*, 2017, **139**, 57–63.

14 V. K. Patle, R. Kumar, A. Sharma, N. Dwivedi, D. Muchhala, A. Chaudhary, Y. Mehta, D. P. Mondal and A. K. Srivastava, Three dimension phenolic resin derived carbon-cnts hybrid foam for fire retardant and effective electromagnetic interference shielding, *Composites Part C: Open Access*, 2020, **2**, 100020–100030.

15 Z. Wang, T. Yang, Z. Wang, G. Chai and X. Zhang, Polymethyl methacrylate/carbon nanotube composites, *Fire Sci. Technol.*, 2018, **37**(5), 655–657.

16 Z. Jia, X. Xu, X. Yan, Y. Pan and J. Jiang, Effect of ammonium polyphosphate and carbon nanotubes on flame retardancy of high impact polystyrene composites, *J. Nanjing Tech Univ., Nat. Sci. Ed.*, 2021, **43**(2), 184–188.

17 W. Xing, W. Yang, W. Yang and Q. Hu, Functionalized Carbon Nanotubes with Phosphorus- and Nitrogen-Containing Agents: Effective Reinforcer for Thermal, Mechanical, and Flame-Retardant Properties of Polystyrene Nanocomposites, *ACS Appl. Mater. Interfaces*, 2016, **8**(39), 26266–26274.

18 D. Wang, Q. Zhang, K. Zhou, W. Yang, Y. Hu and X. Gong, The influence of manganese-cobalt oxide/graphene on reducing fire hazards of poly(butylene terephthalate), *J. Hazard. Mater.*, 2014, **278**, 391–400.

19 A. A. Bogdanov, Processes of aggregation of fullerene C_{60} in polymer–fullerene composites, *Phys. Solid State*, 2020, **62**(2), 354–358.

20 A. Penicaud, K. Boubekeur, A. I. Kotov and E. B. Yagubskii, Novel infinite three-dimensional network of neutral fullerene molecules in $(C_{60})_8$(twin-TDAS)$_6$, *Acta Crystallogr., Sect. B: Struct. Sci.*, 2010, **56**(3), 497–500.

21 P. V. Redkin and R. A. Ganeev, Simulation of resonant high-order harmonic generation in a three-dimensional fullerenelike system by means of a multiconfigurational time-dependent hartree-fock approach, *Phys. Rev. A*, 2010, **81**(6), 399–403.

22 W. Khuntawee, T. Sutthibutpong, S. Phongphanphanee, M. Karttunen and J. Wong-Ekkabut, Molecular dynamics study of natural rubber-fullerene composites: connecting microscopic properties to macroscopic behavior, *Phys. Chem. Chem. Phys.*, 2019, **21**(35), 19403–19413.

23 J. Du, Z. Jin, C. A. Wilkie and J. Wang, An XPS investigation of thermal degradation and charring on PMMA clay nanocomposites, *Polym. Degrad. Stab.*, 2002, **77**(3), 377–381.

24 B. Yang, L. Wang, Y. Guo, Y. Zhang and L. Tian, Synthesis of a novel phosphate-containing highly transparent PMMA copolymer with enhanced thermal and flame retardant properties, *Polym. Adv. Technol.*, 2020, **31**(3), 472–481.

25 J. Lee, C. Lee, E. Osawa and K. H. Lee, Dynamic behavior of C_{60} fullerene in carbon nanopeapods: tight-binding molecular dynamics simulation, *Bull. Korean Chem. Soc.*, 2019, **40**(7), 724–728.

26 R. Tupciauskas, I. Irbe, A. Janberga and E. Buksans, Moisture and decay resistance and reaction to fire properties of self-binding fibreboard made from steam-exploded grey alder wood, *Wood Mater. Sci. Eng.*, 2017, **12**(2), 63–71.

27 A. K. Sen, G. Litak, K. D. Edwards, C. Finney, C. S. Daw and R. M. Wagner, Characteristics of cyclic heat release variability in the transition from spark ignition to HCCI in a gasoline engine, *Appl. Energy*, 2011, **88**(5), 1649–1655.

28 H. Hu, X. Wang, J. Wang, L. Wan, F. Liu, H. Zheng, R. Chen and C. Xu, Preparation and properties of graphene nanosheets-polystyrene nanocomposites *via in situ* emulsion polymerization, *Chem. Phys. Lett.*, 2010, **484**(4), 247–253.

29 T. Kulia, S. Bhadra and D. Yao, Recent advances in graphene based polymer composites, *Prog. Polym. Sci.*, 2010, **35**(11), 1350–1375.

30 S. Kumar and S. K. Pattanayek, Semi-flexible polymer engendered aggregation/dispersion of fullerene (C_{60}) nanoparticles: an atomistic investigation, *Chem. Phys. Lett.*, 2018, **701**, 22–29.

31 L. Li, H. Tang, H. Wu, G. Lu and X. Yang, Effects of fullerene solubility on the crystallization of poly(3-hexylthiophene) and performance of photovoltaic devices, *Org. Electron.*, 2009, **10**(7), 1334–1344.